EPJ Web of Conferences **164**, 06005 (2017) DOI: 10.1051/epjconf/201716406005
ICNFP 2016

Results from the RHIC Beam Energy Scan

A. Taranenko[1,a]

[1] *National Research Nuclear University MEPhI (Moscow Engineering Physics Institute), Kashirskoe highway 31, Moscow, 115409, Russia*

Abstract. The first phase of the Beam Energy Scan (BES-I) program at the Relativistic Heavy Ion Collider (RHIC) is based on Au+Au collision data collected between 2010 and 2014 at center-of-mass energies $\sqrt{s_{\rm NN}}$=7.7, 11.5, 14.5, 19.6, 27, and 39 GeV. The BES-I program has four physics goals: search for the turning off of the signatures of the Quark Gluon Plasma (QGP), the search for the possible first-order phase transition between hadronic gas and QGP, the search for the possible critical end point and the study of the transport properties of the strongly interacting matter as a function of the temperature T and baryon chemical potential μ_B. In this article, we briefly review and discuss the main results and their understanding from the BES-I program and future plans for the BES-II program (2019-2020).

1 Introduction

The first decade of RHIC running (2000-2010) at top energy of $\sqrt{s_{\rm NN}}$ =200 GeV has established the existence of a strongly coupled Quark Gluon Plasma (sQGP), a new state of nuclear matter with partonic degrees of freedom [1, 2] and with low specific shear viscosity η/s, i.e. the ratio of shear viscosity η to entropy density s [3, 4]. The left panel of Figure 1 shows a cartoon of the phase diagram of nuclear matter. Lattice QCD calculations [5] indicate that the quark-hadron transition is a smooth crossover at top RHIC energies and above (small μ_B). The possible region of a first order phase transition is expected at larger values of μ_B (lower beam energies), suggesting the existence of a critical end point (CEP) [6]. Thus, a current strategy for experimental mapping of the phase diagram is centered on beam energy scans, which sample reaction trajectories with the broadest possible range of μ_B and T values. The RHIC BES-I program (2010-2014) has four physics goals [7–9]: search for the turning off of the signatures of the QGP well established at top RHIC energies, the search for the possible first-order phase transition between hadronic gas and QGP and for critical end point, and the study of the transport properties of the strongly interacting matter: e.g $\eta/s(T,\mu_B)$. The $\sqrt{s_{\rm NN}}$ energies from BES-I program (200-7.7 GeV) correspond to baryon chemical potentials (μ_B) in the range 25 to about 400 MeV [8]. The midrapidity transverse-energy distributions, $dE_T/d\eta$, for Au+Au collisions at $\sqrt{s_{\rm NN}}$ = 7.7-200 GeV were measured by PHENIX collaboration [10]. The right panel of Fig. 1 shows estimates of the initial energy density times the formation time of a QGP τ_0 for various Au-Au collision centralities. Lattice calculations show that the QGP should form when the energy density gets much higher than 0.6 GeV/fm^3 [11]. For τ_0 = 1 fm, for the Au+Au collisions at $\sqrt{s_{\rm NN}}$=7.7 GeV

[a] e-mail: AVTaranenko@mephi.ru

can be expected to create a QGP according to this estimate. Even for $\tau_0 = 2$ fm, the central 7.7 GeV collisions would reach energy densities high enough for QGP formation.

2 Search for the turning off of the signatures of the QGP

Key evidence for the formation of a strongly coupled Quark Gluon Plasma (sQGP) in Au+Au collisions at top RHIC energies was the observation of jet quenching and large azimuthal anisotropic flow signals for all produced particles [1, 2]. The results of STAR measurements show that the strong suppression of high p_T charged particles, as indicated by comparisons of binary scaled yields, is no longer evident in Au+Au collisions at $\sqrt{s_{\rm NN}} < 14.5\ GeV$ for any centrality [12]. This may indicate that hard scattering effects become rare at lower beam energies, as the high-p_T regions are much less populated [8].

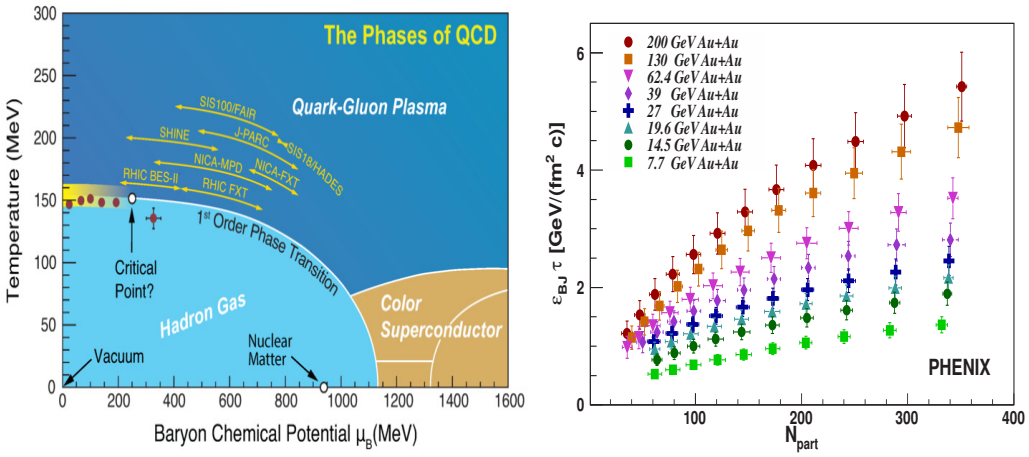

Figure 1. Left: Schematic view of QCD phase diagram plotted as temperature T versus baryon chemical potential μ_B. Various details, as the position of the critical end point and order of the phase transition curve are highly uncertain. The figure is taken from [9]. Right: Estimates of the initial energy density for a variety of energies time the formation time. Figure from [10].

The anisotropic flow, as manifested by the anisotropic emission of particles in the plane transverse to the beam direction, is one of the important observables sensitive to the transport properties of sQGP: the equation of state, the speed of sound, and the value of specific shear viscosity η/s. The azimuthal anisotropy of produced particles can be quantified by the Fourier coefficients v_n in the expansion of the particles' azimuthal distribution as: $dN/d\phi \propto 1 + \sum_{n=1} 2v_n \cos(n(\phi - \Psi_n))$ [13–15], where n is the order of the harmonic, ϕ is the azimuthal angle of particles of a given type, and Ψ_n is the azimuthal angle of the nth-order event plane. The $n^{\rm th}$-order flow coefficients v_n can be calculated as $v_n = \langle \cos[n(\varphi - \Psi_n)] \rangle$, where the brackets denote an average over particles and events. Relativistic viscous hydrodynamics has been successful in describing the observed flow anisotropy v_n for the produced particles in the collision of heavy-ion systems like Au+Au at 200 GeV (RHIC) and Pb+Pb at 2.7 TeV (LHC) [3, 4, 16]. In this model framework, the values of the coefficients v_n (for $p_T < 3 - 4$ GeV/c) have been attributed to an eccentricity-driven hydrodynamic expansion of the plasma produced in the collision zone. That is, a finite eccentricity moment ε_n drives uneven pressure

gradients in- and out of the event plane ψ_n, and the resulting expansion leads to the anisotropic flow of particles about this plane. The event-by-event geometric fluctuations in its initial density distribution are found to be responsible for finite elliptic flow signal v_2 in the collisions with almost zero impact parameter, and the presence of odd harmonic moments in the initial geometry ε_n and final momentum anisotropy v_n [14, 15]. The proportionality constant between v_n and ε_n is found to be sensitive to the transport properties of the matter such as as the equation of state and the specific shear viscosity η/s. The shear viscosity suppresses higher order harmonic flow coefficients $v_{n>2}$ more strongly than the elliptic flow signal v_2. The v_n data at top RHIC energies and LHC seem to follow the "acoustic scaling" for anisotropic flow, which suggests that viscous corrections to v_n/ε_n grow exponentially as n^2 and $1/(\bar{R}T)$ [17–19]:

$$\frac{v_n(p_T, \text{cent})}{\varepsilon_n(\text{cent})} \propto \exp\left[-n^2\beta'\right],\ \beta' \propto \frac{\eta}{s}\frac{1}{\bar{R}T} \propto \frac{\eta}{s}\frac{1}{(dN_{ch}/d\eta)^{1/3}} \tag{1}$$

where T is the temperature, $\bar{R}$ is the transverse size of the collision zone and ε_n is the n-th order eccentricity moment. For a given harmonic number n, this equation indicates a characteristic linear dependence of $\ln(v_n/\varepsilon_n)$ on $1/(\bar{R}T)$, with a slope proportional to η/s [17–19]. The dimensionless size $\bar{R}T$ is approximately proportional to $(dN_{ch}/d\eta)^{1/3}$, where $dN_{ch}/d\eta$ is the charge particle multiplicity density [20].

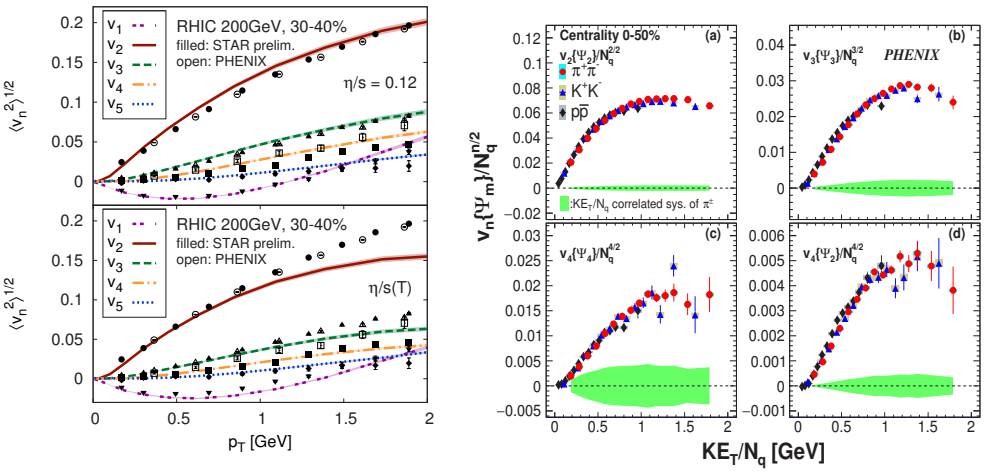

Figure 2. Left: Comparison of viscous hydro calculations and $v_n(p_T)$ data for charged hadrons at top RHIC energy that can be used to better constrain the temperature dependence of η/s. The figure is taken from [3]. Right: Quark-number (n_q) scaling for 0-50% central Au+Au collisions at $\sqrt{s_{\rm NN}}$ = 200 GeV, where n_q is the constituent valence quark number of each hadron and KE_T is the transverse kinetic energy of the hadron [22].

The data for top RHIC energy show that, for a given centrality, $v_{n>1}$ for all observed hadrons scale to a single curve when plotted as $v_n/n_q^{n/2}$ versus KE_T/n_q, where n_q is the number of constituent quarks in a given hadron species and $KE_T = m_T - m_0$ is the transverse kinetic energy for these hadrons [21, 22]. The observed scaling may indicate that the bulk of the anisotropic flow at top RHIC energies is partonic, rather than hadronic. Lowering the collision energy and studying the energy dependence of anisotropic flow allows a search for the onset of the transition to a phase with partonic degrees of freedom at an early stage of the collision.

Figure 3(left) shows the p_T dependence of v_2 of charged hadrons calculated from the four-particle cumulant method measured for several centralities and for energies ranging from 7.7 GeV up to 2.76 TeV[23]. It is striking how little the elliptic flow signal for inclusive charged hadron changes over such a wide range of energies and initial energy densities: the energy changes by a factor 400 and initial energy density changes by nearly a factor of 10. Figure 3(right) shows quark-number (n_q) scaled elliptic flow, v_2/n_q versus $(m_T - m_0)/n_q$, for identified particles produced in 0-80% central Au+Au collisions at $\sqrt{s_{\rm NN}}$ = 7.7-62.4 GeV as published by STAR collaboration [24]. This work shows that the scaling holds separately for most of the particles and anti-particles withing 10-15%. The ϕ meson may not follow the trend of the other identified hadrons at 7.7 and 11.5 GeV, but more data are needed before any conclusions can be drawn. Hybrid model calculations show that the weak dependence of $v_2(p_T)$ on the beam energy may result from the interplay of the hydrodynamic and hadronic transport phase [26]. The trianglular flow v_3 is more sensitive to the viscous damping and might be an ideal observable to probe the formation of a QGP and the pressure gradients in the early plasma phase.

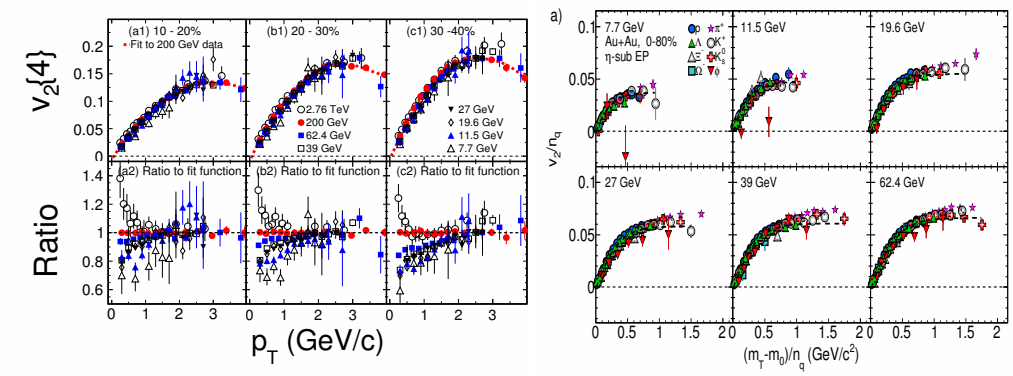

Figure 3. Left: The variation of $v_2(p_T)$ for charged hadrons produced at mid-rapidity from 7.7 GeV up to 2.76 TeV [23]. Right: Quark-number (n_q) scaled elliptic flow, v_2/n_q versus $(m_T - m_0)/n_q$, for identified particles produced in 0-80% central Au+Au collisions at $\sqrt{s_{\rm NN}}$ = 7.7-62.4 GeV, where n_q is the constituent valence quark number of each hadron and $(m_T - m_0)$ is the transverse kinetic energy of the particle [24].

Figure 4 left shows the variation of $v_3^2\{2\}$ for charged hadrons produced at mid-rapidity from 7.7 GeV up to 2.76 TeV for different bins in collision centrality [25]. At low energies $\sqrt{s_{\rm NN}} < 14.5\ GeV$, the $v_3^2\{2\}$ become consistent with zero in 50-60% peripheral collisions. This result is consistent with the idea of absence of a low viscosity QGP phase in low energy peripheral collisions [26]. For more central collisions, the values of $v_3^2\{2\}$ are positive and change little from 19.6 GeV to 7.7 GeV. For the energies above 19.6 GeV, the values of $v_3^2\{2\}$ linearly increase with the $log(\sqrt{s_{\rm NN}})$ for all bins in collision centrality [25]. Figure 4 right shows the preliminary data from STAR collaboration for v_3 of identified charged hadrons from Au+Au collisions at $\sqrt{s_{\rm NN}}$ = 200 GeV (upper panels) and 39 GeV (lower panels) [27]. The left panels represent the results for particles and right panels for anti-particles. For 200 GeV the measured v_3 values follow the $v_3/n_q^{3/2}$ versus $(m_T - m_0)/n_q$ scaling. However, for 39 GeV data one can see that the scaling is not so perfect.

The left panel of Fig. 5 shows the preliminary STAR data for the $\sqrt{s_{\rm NN}}$ dependence of the p_T integrated v_n of charged hadrons from 0-40% central Au+Au collisions [19]. It shows an essentially monotonic trend for v_2, v_3 and v_4 with $\sqrt{s_{\rm NN}}$ as might be expected for a temperature increase as $\sqrt{s_{\rm NN}}$ increases [19]. The same authors applied the "acoustic scaling" to v_n data in order to estimate the $\sqrt{s_{\rm NN}}$ dependence of η/s. Using the observation that ε_n changes very slowly with beam energy and

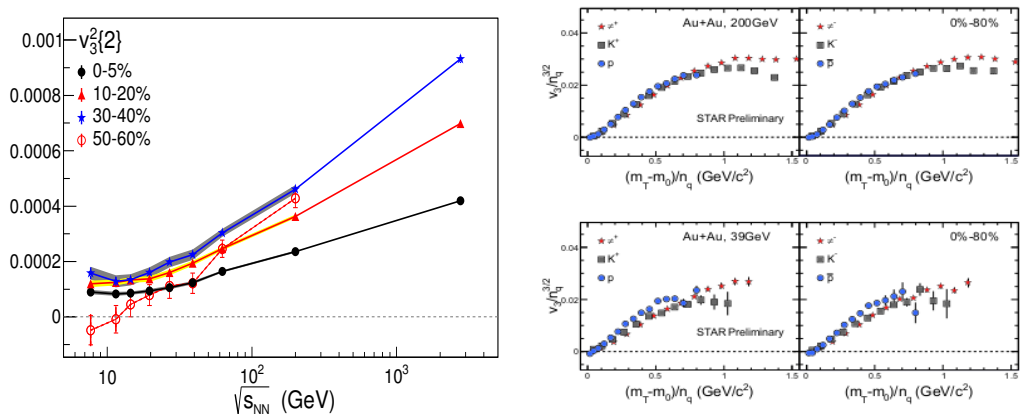

Figure 4. Left: The variation of $v_3^2\{2\}$ for charged hadrons produced at mid-rapidity from 7.7 GeV up to 2.76 TeV [23] for different bins in collision centrality. The figure is taken from [25] Right: Quark-number (n_q) scaled triangular flow, $v_3/n_q^{3/2}$ versus $(m_T - m_0)/n_q$, for charged pions, kaons and (anti)protons emerged from 0-80% central Au+Au collisions at $\sqrt{s_{NN}}$ = 200 GeV (top panels) and at $\sqrt{s_{NN}}$ = 39 GeV (bottom panels). The left panels represent the results for particles and right panels for anti-particles. The figure is taken from [27].

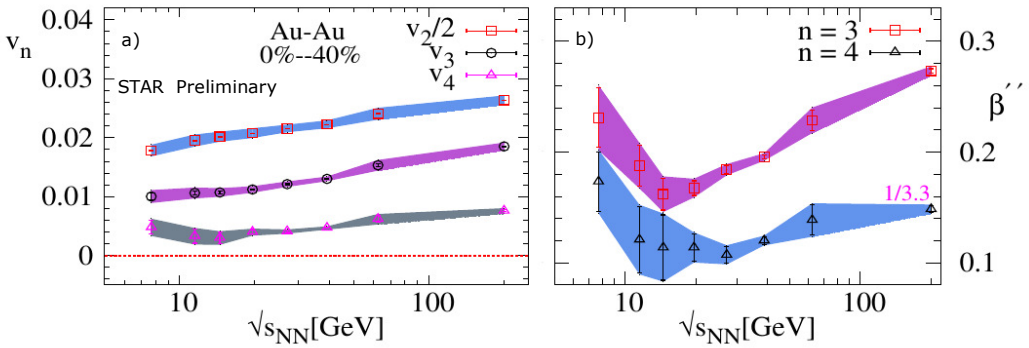

Figure 5. $\sqrt{s_{NN}}$ dependence of the p_T -integrated v_n (left panel) and the estimated viscous coefficient $\beta^{"} \propto \eta/s$ (right panel). Results are shown for 0-40% central Au+Au collisions; the shaded lines are the systematic uncertainty. The figure is taken from [19].

the measurements for two different harmonics$n$ and $n^{'}$ $(n \neq n^{'})$ the Eq.1 can be simplified [19] to the viscous coefficient $\beta^{"} \propto (\eta/s) \propto (dN_{ch}/d\eta)^{1/3} ln(v_n^{1/n}/v_{n^{'}}^{1/n^{'}})$. The right panel of Fig. 5 shows the $\sqrt{s_{NN}}$ dependence of the viscous parameter $\beta^{"}$ extracted from the $ln(v_3^{1/3}/v_2^{1/2})$ and $ln(v_4^{1/4}/v_2^{1/2})$ results from the left panel of Fig. 5. In contrast to v_n, the excitation function of the viscous parameter $\beta^{"}$ shows a non-monotonic behaviour over the same beam energy range. A similar non-monotonic trend for η/s has been observed in the hybrid viscous hydrodynamical calculations [28], tuned to describe the STAR BES-I v_2 data.

3 Search for the first-order phase transition

The next BES-I goal is to search for the predicted first-order phase transition [12, 13] between hadronic and QGP phases. Such a transition can also be characterized by a dramatic drop in the pressure, or a softening of the Equation of State (EOS) [14, 15]. The signals like anisotropic flow are very promising due to their sensitivity to EOS. The directed flow (v_1) can probe the very early stages of the collision as it is generated during the passage time of the two colliding nuclei [29]. Both hydrodynamic [21, 22] and transport model [23, 24] calculations indicate that the directed ow of charged particles, especially baryons at midrapidity, is very sensitive to the equation of state. The slope of the rapidity dependence dv_1/dy close to mid-rapidity is a convenient way to characterize the overall magnitude of the directed flow signal. The left panel of Fig. 6 shows slope of net-proton and net-kaon directed flow (v1) as a function of $\sqrt{s_{\rm NN}}$ measured by the STAR. The non-monotonic behavior with a double sign-change in dv_1/dy and with the minimum around $\sqrt{s_{\rm NN}}$=14.5 GeV is observed for net-protons. The slope of net-kaon directed flow shows a monotonic decrease trend with decreasing energy. The observed double sign-change in dv_1/dy for net-protons could be related to the softening of equation-of-state due to the first order phase transition. However, the final-state interaction effects may also play an important role in the observed v_1 signals and overall agreement between theory and data is very poor.

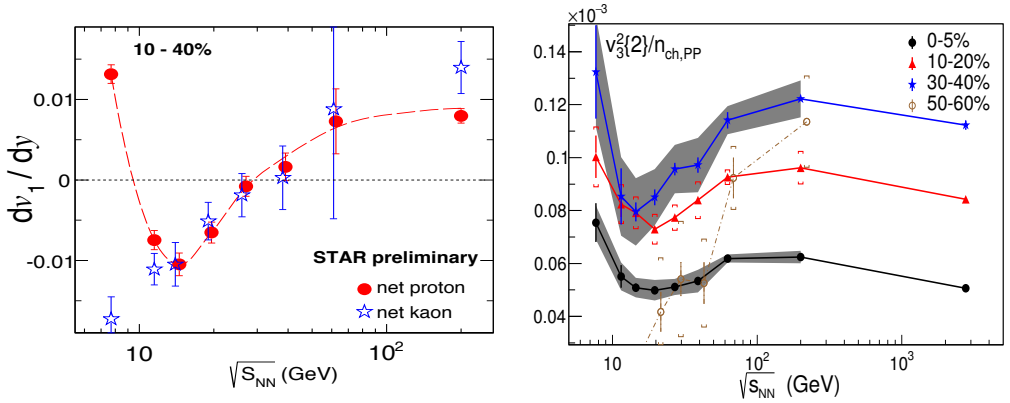

Figure 6. Left: Beam Energy dependence of directed flow slope dv_1/dy near mid-rapidity for net-protons and net-kaons from 10-40% central Au+Au collisions measured by STAR. The figure is taken from [9] Right: Beam energy dependence of $v_3^2\{2\}$ of charged hadrons divided by the mid-rapidity, charged particle multiplicity, pseudo-rapidity density per participant pair in Au+Au and Pb+Pb (2.76 TeV) collisions. The figure is taken from [25].

The next promising probe which may be sensitive to the pressure produced at early stage is the $v_3^2\{2\}$ signal, please see the previous section. The right panel of Fig. 6 shows $\sqrt{s_{\rm NN}}$ dependence of the $v_3^2\{2\}$ for charged hadrons from Au+Au collisions (data from left panel of Fig. 4) scaled by the charged particle multiplicity per participant pair $n_{ch,\rm PP} = \frac{2}{N_{\rm part}} dN_{ch}/d\eta$ for four bins in collision centrality [25]. The central and semi-central collisions data exhibit a local minimum in the $\sqrt{s_{\rm NN}}$ range around 15-20 GeV which is absent for peripheral collisions. This is the consequence of a relatively flat trend for $v_3^2\{2\}$ and monotonically increasing trend for the $n_{ch,\rm PP}$ in the energy range 7.7 < $\sqrt{s_{\rm NN}}$ < 20 GeV. If the general increase of $v_3^2\{2\}$ is driven by ever increasing pressure gradients in ever denser systems at higher energies, then the local minimum in $v_3^2\{2\}/n_{\rm ch,PP}$ could be an indication of an anomalously low

pressure inside the matter created in collisions with energies near 15-20 GeV, where a minimum is also observed for the slope of net-proton directed flow [25]. The interpretation of data in this energy regime is complicated by changes in meson to baryon ratio, baryon stopping, non-flow effects and fluctuations, and longer passing time at lower energies [25].

4 Search for the QCD critical end point

A common strategy for locating the critical end point (CEP) is to scan the phase diagram by varying the $\sqrt{s_{\rm NN}}$, and look for an increase/divergence or a non-monotonic behavior of experimental observables sensitive to the correlation length (ξ) [31]. Large fluctuations in the event-by-event distributions of conserved quantities, such as net-charge, net-baryon number, and net-strangeness have been proposed as possible experimental signatures of the QCD CEP [36]. The moments of these distributions can be related to the correlation length (ξ) and can be directly connected to the susceptibility of the system computed in Lattice QCD [32, 33]. The higher-order moments are predicted to be even more sensitive to the CEP since they are proportional to higher powers of the correlation length. The STAR experiment has measured various order fluctuations of net-proton ($N_p - N_{\bar{p}}$, proxy for net-baryon), net-charge and net-kaon (proxy for net-strangeness) numbers in the Au+Au collisions at $\sqrt{s_{\rm NN}}$=7.7-200 GeV [7].

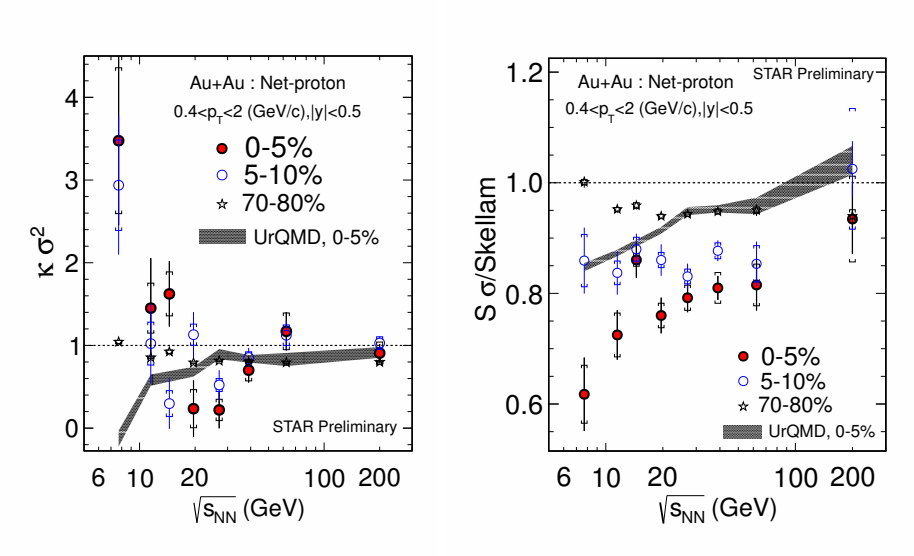

Figure 7. Left: $\sqrt{s_{\rm NN}}$ dependence of $\kappa\sigma^2$ of net-proton distributions and Right: $S\sigma$ divided by Skellam (Poisson) expectations for 0-5%, 5-10% and 70-80% centralities of Au+Au collisions measured by STAR. The experimental data is compared with Poisson expectations (dashed lines) and the UrQMD transport model calculations (shade bands). The protons and anti-protons numbers are measured with transverse momentum $0.4 < p_{\rm T} < 2$ GeV/c and at mid-rapidity $|y| < 0.5$. The figure is taken from [7].

The moment products ($S\sigma$ and $\kappa\sigma^2$) are related to the ratio of baryon number susceptibilities, $S\sigma \sim \chi_B^{(3)}/\chi_B^{(2)}$ and $\kappa\sigma^2 \sim \chi_B^{(4)}/\chi_B^{(2)}$ [36, 37]. Here, σ, S and κ are the variance, skewness and kurtosis (respectively) of the event-by-event net-proton multiplicity distributions. Figure 7 left shows

the efficiency corrected $\kappa\sigma^2$ of net-proton distributions as a function of $\sqrt{s_{NN}}$ for 0-5%, 5-10% and 70-80% centralities of Au+Au collisions measured by STAR [7]. The $\kappa\sigma^2$ shows a clear non-monotonic variation with $\sqrt{s_{\rm NN}}$ for 0-5% centrality with a minimum around 20 GeV. with a steep rise as the beam energy is scanned further down, ending with a value about 2 standard errors above the baseline at 7.7 GeV. The $\kappa\sigma^2$ results are qualitatively consistent with a QCD based model including a critical point [21]. The new data from RHIC BES-II should help to check the prediction that $\kappa\sigma^2$ moments will return to unity at $\sqrt{s_{\rm NN}} < 7.7$ GeV as they do at high $\sqrt{s_{\rm NN}}$. The right panel of Fig. 7 shows the $S\sigma$ of net-proton distributions divided by the skellam baselines [7] as a function of $\sqrt{s_{\rm NN}}$ for three centralities measured by STAR. For 0-5% centrality, the $S\sigma$/Skellam shows significantly deviate below unity and monotonically decrease with decreasing energies except for showing a peak at 14.5 GeV. The results from UrQMD model without critical point, show a monotonic decreasing trend as a function of $\sqrt{s_{\rm NN}}$ and can not reproduce the structures observed in $\kappa\sigma^2$ and $S\sigma$/Skellam of net-proton distributions measured by STAR.

An emitting system produced in the vicinity of the critical end point would also be subject to the influence of a divergence in the compressibility of the medium, resulting in a collateral increase in the emission duration [39]. One can expect to see the non-monotonic dependence in the excitation functions ($\sqrt{s_{\rm NN}}$) for the difference between the Gaussian emission source radii ($R^2_{\rm out} - R^2_{\rm side}$), related to the time duration of emission [40]. The left panel of Fig. 8 shows the $\sqrt{s_{\rm NN}}$ dependence of the charged pion femtoscopy parameters ($R^2_{\rm out} - R^2_{\rm side}$) for 0-5%, 5-10%, 10-20%, 30-40%, 40-50% and 50-60% central Au+Au and Pb+Pb collisions from 7.7 GeV to 2.76 TeV. The observed non-monotonic behavior of ($R^2_{\rm out} - R^2_{\rm side}$) may indicate an increase in the emission duration in the vicinity of the peak at $\sqrt{s_{\rm NN}}$ = 20-40 GeV. The magnitude of the peaks decrease with increasing centrality and positions of the peaks shift to lower values of $\sqrt{s_{\rm NN}}$ with an increase in centrality, the width of the distributions increases with centrality. R.A. Lacey has attributed these qualitative patterns for ($R^2_{\rm out} - R^2_{\rm side}$) distributions to the Finite-Size Scaling (FSS) effects expected for the deconfinement phase transition [40]. A finite-size scaling (FSS) analysis of these data suggests a second order phase transition with the estimates $T^{cep} \sim 165MeV$ and $\mu_B^{cep} \sim 95MeV$ for the location of the critical end point. The first interesting observation is that all ($R^2_{\rm out} - R^2_{\rm side}$) data points for different values of $\sqrt{s_{\rm NN}}$ and centralities (from the left panel of Fig. 8) will collapse onto a single curve in the FSS scaled variables, see the right panel of Fig. 8. The second observation is that the same parameters: $T^{cep} \sim 165MeV$ and $\mu_B^{cep} \sim 95MeV$ will work for recent STAR measurements of the excitation function for the moment products $S\sigma$ and $\kappa\sigma^2$ of the event-by-event net-proton multiplicity distributions [41]. The data for 7 centrality bins will also collapse onto a single curve in the FSS scaled variables. The change in parameter of μ_B^{cep} from 95 MeV to 205 MeV will break the scaling for $S\sigma$ and $\kappa\sigma^2$ [41].

5 Plans for RHIC Beam Energy Scan Phase-II

The STAR Collaboration has planned a second phase of the Beam Energy Scan program at RHIC (BES-II), scheduled for 2019-2020, to explore the high baryon density region of the QCD phase diagram [42, 43]. The upgrades for STAR detector and RHIC accelerator have been started. The stochastic electron cooling technique and long beam bunches will be applied to accelerate gold beam, which will improve the luminosity by a factor about 10 at $\sqrt{s_{\rm NN}}$ =19.6 GeV to 25 at $\sqrt{s_{\rm NN}}$ =7.7 GeV compared to BES-I. The proposed Fixed-Target program (FXT)[44], which uses only one beam on an internal target will allows STAR to reach higher μ_B (μ_B=720 MeV for $\sqrt{s_{\rm NN}} = 3GeV$) with high luminosity. There are three detector upgrades are ongoing at STAR: the iTPC upgrade [45], the Event Plane Detector (EPD) upgrade [46] and the eTOF upgrade [47], see left panel of Fig. 9. The inner TPC (iTPC) of STAR[45] is being upgraded to improve the energy loss dE/dx resolution, momentum

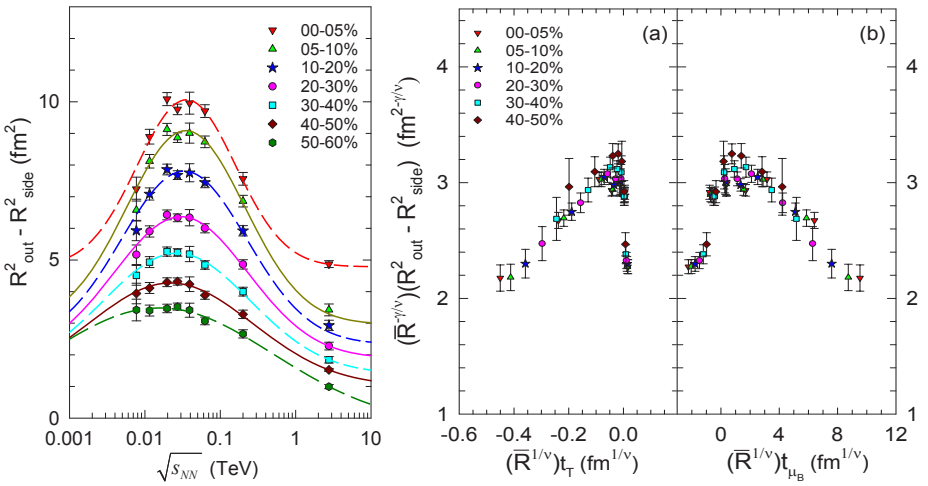

Figure 8. Left: Pion femtoscopy parameters ($R^2_{\rm out} - R^2_{\rm side}$) vs. $\sqrt{s_{NN}}$ for 0-5%, 5-10%, 10-20%, 30-40%, 40-50% and 50-60% central Au+Au and Pb+Pb collisions for $m_T = 0.26$ GeV and 0.29 GeV. Right: (a) $\bar{R}^{-\gamma/\nu}\times(R^2_{\rm out}-R^2_{\rm side})$ vs. $\bar{R}^{1/\nu} \times t_T$. (b) $\bar{R}^{-\gamma/\nu} \times (R^2_{\rm out} - R^2_{\rm side})$ vs. $\bar{R}^{1/\nu} \times t_{\mu_B}$. The $(R^2_{\rm out} - R^2_{\rm side})$ values are the same as those in Left panel. The figures are taken from [40].

resolution, the pseudo-rapidity acceptance from $|\eta| < 1$ to $|\eta| < 1.5$ and acceptance for low p_T particles from 125 MeV/c to 60 MeV/c. The EPD is a new dedicated event-plane and centrality detector placed in the forward rapidity region $2 < |\eta| < 4$. With 16 radial segments and 24 azimuthal segments, the detector will provide precise measurements of both the collision centrality and the event plane for all possible harmonics. The Endcap Time-Of-Flight (eTOF) is the result of a CBM and STAR collaboration [47]; 10% of the full CBM ToF system will be installed on one side of STAR, covering $-1.1 < y < -1.6$, as part the FAIR Phase-0 program. In combination with the new inner TPC sectors, particle identification will now be possible at forward rapidities, see right panel of Fig. 9.

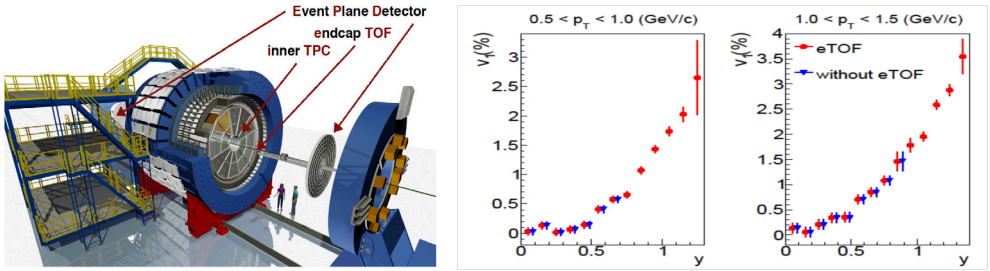

Figure 9. (Color online) Left: Upgrades of the STAR detector for the second phase of beam energy scan at RHIC. Right: The expected improvement in the rapidity dependence of the proton v_1 due to the inclusion of the iTPC and eTOF upgrades for the BES-II [47].

6 Acknowledgment

This work was partially supported by the Ministry of Science and Education of the Russian Federation, grant N 3.3380.2017/4.6, and by the National Research Nuclear University MEPhI in the framework of the Russian Academic Excellence Project (contract No. 02.a03.21.0005, 27.08.2013).

References

[1] K. Adcox *et al.* [PHENIX Collaboration], Nucl. Phys. A **757** (2005) 184
[2] J. Adams *et al.* [STAR Collaboration], Nucl. Phys. A **757** (2005) 102
[3] C. Gale, S. Jeon, B. Schenke, P. Tribedy and R. Venugopalan, Phys. Rev. Lett. **110** (2013) no.1, 012302
[4] U. Heinz and R. Snellings, Ann. Rev. Nucl. Part. Sci. **63** (2013) 123
[5] Y. Aoki, G. Endrodi, Z. Fodor, S. D. Katz and K. K. Szabo, Nature **443** (2006) 675
[6] S. Ejiri, Phys. Rev. D **78** (2008) 074507 ; E. S. Bowman, J. I. Kapusta, Phys. Rev. C **79** (2009) 015202.
[7] X. Luo, Nucl. Phys. A **956** (2016) 75
[8] D. Keane, J. Phys. Conf. Ser. **878** (2017) no.1, 012015.
[9] H. Caines, Nucl. Phys. A **967** (2017) 121.
[10] A. Adare *et al.* [PHENIX Collaboration], Phys. Rev. C **93** (2016) no.2, 024901
[11] A. Bazavov *et al.* [HotQCD Collaboration], Phys. Rev. D **90** (2014) 094503
[12] L. Adamczyk *et al.* [STAR Collaboration], arXiv:1707.01988 [nucl-ex].
[13] S. Voloshin and Y. Zhang, Z. Phys. C **70** (1996) 665
[14] S. A. Voloshin, A. M. Poskanzer and R. Snellings, arXiv:0809.2949 [nucl-ex].
[15] R. Snellings, J. Phys. G **41** (2014) no.12, 124007
[16] R. Derradi de Souza, T. Koide and T. Kodama, Prog. Part. Nucl. Phys. **86** (2016) 35
[17] R. A. Lacey, A. Taranenko, J. Jia, D. Reynolds, N. N. Ajitanand, J. M. Alexander, Y. Gu and A. Mwai, Phys. Rev. Lett. **112** (2014) no.8, 082302
[18] R. A. Lacey, D. Reynolds, A. Taranenko, N. N. Ajitanand, J. M. Alexander, F. H. Liu, Y. Gu and A. Mwai, J. Phys. G **43** (2016) no.10, 10LT01
[19] N. Magdy [STAR Collaboration], J. Phys. Conf. Ser. **779** (2017) no.1, 012060.
[20] R. A. Lacey *et al.* , arXiv:1601.06001 [nucl-ex].
[21] R. A. Lacey and A. Taranenko, PoS CFRNC **2006** (2006) 021
[22] A. Adare *et al.* [PHENIX Collaboration], Phys. Rev. C **93** (2016) no.5, 051902
[23] L. Adamczyk *et al.* [STAR Collaboration], Phys. Rev. C **86** (2012) 054908
[24] L. Adamczyk *et al.* [STAR Collaboration], Phys. Rev. C **88** (2013) 014902
[25] L. Adamczyk *et al.* [STAR Collaboration], Phys. Rev. Lett. **116** (2016) no.11, 112302
[26] J. Auvinen and H. Petersen, Phys. Rev. C **88** (2013) no.6, 064908
[27] X. Sun [STAR Collaboration], J. Phys. Conf. Ser. **535** (2014) 012005.
[28] I. A. Karpenko, P. Huovinen, H. Petersen and M. Bleicher, Phys. Rev. C **91** (2015) no.6, 064901
[29] S. Singha, P. Shanmuganathan and D. Keane, Adv. High Energy Phys. **2016** (2016) 2836989
[30] M. Asakawa, S. Ejiri and M. Kitazawa, Phys. Rev. Lett. **103** (2009) 262301
[31] M. Asakawa *et al.*, Phys. Rev. Lett. **103**, 262301 (2009); M. A. Stephanov, Phys. Rev. Lett. **102**, 032301 (2009).

[32] A. Bazavov *et al.*, Phys. Rev. Lett. **109**, 192302 (2012); S. Borsanyi *et al.*, Phys. Rev. Lett. **111**, 062005 (2013); P. Alba *et al.*, Phys. Lett. B **738**, 305 (2014). F. Karsch *et al.*, Nucl. Phys. A, these proceedings. [arXiv:1512.06987].
[33] M. Cheng *et al.*, Phys. Rev. D **79**, 074505 (2009). A. Bazavov, *et al.*, Phys. Rev. D **86**, 034509 (2012).
[34] L. Adamczyk *et al.* [STAR Collaboration], Phys. Rev. Lett. **112** (2014) 032302
[35] M. A. Stephanov, K. Rajagopal and E. V. Shuryak, Phys. Rev. D **60** (1999) 114028
[36] M. A. Stephanov, Phys. Rev. Lett. **102** (2009) 032301
[37] C. Athanasiou, K. Rajagopal and M. Stephanov, Phys. Rev. D **82** (2010) 074008
[38] M. A. Stephanov, Phys. Rev. Lett. **107** (2011) 052301
[39] M. A. Lisa, S. Pratt, R. Soltz and U. Wiedemann, Ann. Rev. Nucl. Part. Sci. **55** (2005) 357
[40] R. A. Lacey, Phys. Rev. Lett. **114** (2015) no.14, 142301
[41] R. A. Lacey, P. Liu, N. Magdy, B. Schweid and N. N. Ajitanand, arXiv:1606.08071 [nucl-ex].
[42] STAR Note 598. https://drupal.star.bnl.gov/STAR/starnotes/public/sn0598
[43] C. Yang [STAR Collaboration], Nucl. Phys. A **967** (2017) 800.
[44] K. Meehan [STAR Collaboration], Nucl. Phys. A **967** (2017) 808
[45] STAR Note 619. https://drupal.star.bnl.gov/STAR/starnotes/public/sn0619
[46] STAR Note 666. https://drupal.star.bnl.gov/STAR/starnotes/public/sn0666
[47] [STAR Collaboration and CBM eTOF Group], arXiv:1609.05102 [nucl-ex].